XVI International Conference on Durability of Building Materials and Components
DBMC 2023, China
K.F. Li and D.P. Fang (Eds)

Oxygen Diffusion Property of Fatigue Damaged Concrete under Drying-wetting Cycle

Zhilu Jiang, Sheng Hong, Chuanqing Fu* and Wenjie Yan

College of Civil Engineering, Zhejiang University of Technology, Hangzhou, China,
zljiang@zjut.edu.cn (Z. Jiang), 13758235809@163.com (S. Hong), chuanqingfu@126.com (C. Fu),
670769874@qq.com (W. Yan)

Abstract. *Oxygen diffusion has an important influence on the corrosion process of reinforced concrete structures. In the marine environment, concrete is subject to both fatigue loads and periodic drying-wetting conditions. In this study, the oxygen diffusion performance of damaged concrete due to fatigue is studied under drying-wetting cycle condition, which is of great significance to the development of concrete durability theory. The pore structures of concrete specimens with different damage degrees after drying-wetting cycle were measured by nuclear magnetic resonance (NMR). The effects of drying-wetting cycle and damage degree on pore structure were studied, and the oxygen diffusivity of damaged concrete before and after drying-wetting cycle was compared and analyzed. The results show that the pore size distribution curves of concrete specimens move to the smaller pores and the peaks decrease after 28 days of drying-wetting cycle. The proportion of gel pores (< 10 nm) increases and the proportion of medium and large capillary pores (10 - 1000 nm) decreases. After the drying-wetting cycle, the porosity of the damaged concrete specimens all decreased to certain degrees. It shows that the microstructure of the specimen is improved and the internal structure of concrete becomes more complex in the early stage of drying-wetting accelerated erosion. After the drying-wetting cycle, the oxygen diffusivity of all concrete specimens decreased, and the oxygen diffusivity of undamaged concrete decreased the most, about 10 times, but with the increase of damage degree, the reduction effect generally decreased.*

Keywords: *Oxygen diffusion, Drying-wetting cycle, Fatigue damage, Concrete, Nuclear magnetic resonance.*

1 Introduction

Oxygen diffusion in concrete cover affects the corrosion rate of steel bars (Zhou et al. 2018). In the periodic drying and wetting environment, harmful ions and gases are transported into the concrete quickly to reduce the durability of the structure. After drying-wetting cycles, the internal damage of concrete accumulates continuously under sulfate attack environment, which accelerates the performance degradation process. This is mainly due to the effect of erosion products such as ettringite and gypsum (Wang et al. 2012). Under the coupling effect of the drying-wetting cycle and load, the transport rate of chloride ions in concrete is much higher than that under soaking conditions (Fu et al. 2016). Few researches have been conducted to study the effect of the drying-wetting cycle on oxygen transport in concrete.

Concrete is a porous material, and its internal pore structure has an important influence on oxygen transport (Zhou et al. 2021). In practical engineering, the internal pore structure of concrete is affected by the subjected load. The water and chloride ion transport properties in concrete are affected by axial tensile fatigue load. When the maximum load exceeds 30% of the ultimate load, the drying rate and chloride penetration rate in concrete will be significantly

accelerated (Fu et al. 2016, Huang et al. 2017). The ion diffusivity of damaged concrete can reach 20 times that of undamaged concrete (Kurumatani et al. 2017). Therefore, the coupling effect of environment and load should be considered when studying transport performance in concrete. This paper studies the oxygen diffusivity of fatigue-damaged concrete after drying-wetting cycle and also explores the influence of fatigue damage degree and drying-wetting cycle on pore structure.

2 Experimental Method

2.1 Raw Materials and Specimen Preparation

PI 42.5 Portland cement, well-graded river sand, natural gravel with a particle size of 5-20 mm and deionized water were used to produce concrete with mix proportion shown in Table 1. The dimension of the concrete specimens is 130 × 130 × 1200 mm. Four steel bars with a diameter of 12 mm were set at the corner of the specimen, extending 100 mm at both ends for later fatigue loading. The concrete specimens were cured at 20 ± 2 °C and 95% relative humidity for 28 days.

Table 1. Mix design of concrete (kg/m^3)

Cement	Deionized water	River sand	Granite gravel
360	191	720	1081

2.2 Axial Tensile Fatigue Test

The specimens were subjected to fatigue loading as shown in Figure 1. Sine wave load with frequency of 5 Hz and 50,000 cycles was applied. Five specimens with different loading levels (Table 2) were used, and unloaded specimen D1 was set as the reference. The ultimate fatigue strain of concrete specimens is basically a constant when fatigue failure occurs (Wei et al. 2016, Yadav and Thapa 2020). Therefore, the damage index of maximum fatigue strain (Zhu 2003) is used to characterize the damage degree of axial tensile fatigue damage concrete:

$$d = \frac{\varepsilon_r - \varepsilon_0}{\varepsilon_{re} - \varepsilon_0} \tag{1}$$

where ε_r is the fatigue strain of concrete specimens after n fatigue cycles, ε_0 is the fatigue strain of concrete specimens without fatigue damage, and ε_{re} is the cumulative fatigue strain of concrete specimens during fatigue damage.

Table 2. Fatigue load for different specimens

Specimen	Load level	P_{min}（kN）	P_{max}（kN）
D1	0%	-	-
Y1	24%-36%	12	18
Y2	30%-42%	15	21
Y3	36%-48%	18	24
Y4	42%-54%	21	27
Y5	48%-60%	24	30

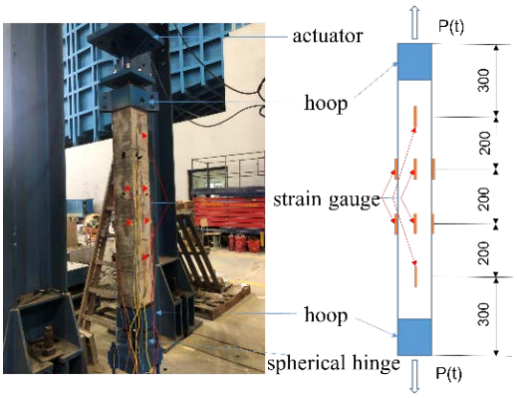

Figure 1. Device for fatigue experiment

2.3 Drying-wetting Test

The specimens without and with fatigue loading were cored with a diameter of 75 mm and a height of 130 mm. To achieve one-dimensional oxygen diffusion, the side of the cylinder was sealed with epoxy resin. For each cylinder, 6 pieces of 20 mm thick discs were cut out for the tests. They were immersed in 3.5% NaCl solution at 20°C. The drying-wetting cycle system with a total of 28 cycles and a cycle of 24 hours is shown in Table 3.

Table 3. Drying-wetting cycle test system

Solution	Cycle period	Drying time	Wetting time	Cycle number
3.5%NaCl	24h	16h (T=50°C， RH=60%)	8h (T=20±2°C)	28

2.4 Oxygen Diffusion Test

Before the oxygen diffusion test, the specimens were dried to constant weight at 45 °C in a vacuum oven. The oxgen diffusivity was tested by an oxygen diffusion device (He et al. 2018). First, the test piece is placed between the two chambers, and then the air inlet valve of one side of the chamber is connected to the oxygen cylinder, and the air inlet of another chamber is connected to the nitrogen cylinder. An initial oxygen concentration gradient is formed between the two chambers so that oxygen diffuses one-dimensionally through the specimen under the action of the concentration gradient(He 2019).

Assuming that the oxygen diffusion in concrete conforms to Fick's law, the oxygen diffusivity D_{fe} is derived from Equation (2).

$$D_{fe} = N \Big/ \left[\left(\int_0^t \partial[C]/\partial[L] \cdot dt \right) \cdot S \right] \tag{2}$$

where $\partial[C]/\partial[L]$ is the concentration gradient of oxygen in the chamber on both sides of the specimen to be tested (mol·m^{-4}); N is the amount of oxygen (mol) passed by the test piece in t time; S is the effective diffusion area (m^2) of oxygen.

Assuming that the oxygen concentration gradient inside the specimen is linearly distributed during the test (Dhir et al. 1995), the oxygen concentration gradient is calculated as

$$\partial[C]/\partial L = \left(C_2 - C_1 \right) \Big/ L = \Delta C / L \tag{3}$$

where L is the thickness of the test piece (m); C_1 is the oxygen concentration ($mol \cdot m^{-3}$) in the chamber of the low-concentration oxygen side at a certain time; C_2 is the oxygen concentration ($mol \cdot m^{-3}$) in the chamber on the side of high-concentration oxygen at the same time.

According to the measured oxygen concentration in the chamber, Equation (3) was used to obtain the concentration gradient at different diffusion time. The oxygen diffusivity was then calculated by Equation (2).

2.5 Low-Field Nuclear Magnetic Resonance Test

To characterize the pore structure of damaged concrete, 40 × 40 × 20 mm samples were cut in the central area of the specimens and then they were vacuum saturated for a low-field nuclear magnetic resonance test.

3 Results and Discussion

The pores in the internal structure of concrete are divided into four parts (Zhang et al. 2016, Zhang et al. 2018): gel pores (< 10 nm), medium capillary pores (10 -100 nm), large capillary pores (100 - 1000 nm) and air voids (> 1000 nm).

3.1 Effect of Damage Degree on Pore Structure

The measured pore size distribution is shown in Figures 2 to Figure 5. The comparison between Figure 2 and Figure 4 shows that before and after the drying-wetting cycles, the gel pores and medium capillary pores with a size range of 1-100 nm are the main components of the pores of concrete with different damage degrees. This result is consistent with the fact that the pore size of concrete is mostly concentrated in the medium pores (Luo and Niu 2019, Niu et al. 2019). As damage degree increases, the trends of volume change of pores large than 100 nm is not obvious. This may be due to the non-uniformity inside the concrete during the preparation of the sample. Because the degree of fatigue load damage is small, and the pore size distribution is mainly concentrated in the pore size range of 1-100 nm. Therefore, the following analysis is mainly based on the medium and small pores in this range.

Figure 2 shows that before the drying-wetting cycles, the pore size corresponding to the peak value of the pore proportion of the concrete is in the range of 10-100 nm, and the peak value of the damaged concrete is greater than that of the undamaged concrete. Figure 3 shows that the pores of the concrete are concentrated in the range of pore size smaller than 100 nm before the drying-wetting cycles. With the increase of damage degree, the pores smaller than 100 nm in concrete increase, indicating that the damage is mainly reflected in the generation and expansion of medium capillary pores. This also confirms that the peak value of damaged concrete in Figure 2 is greater than that of undamaged concrete. When the damage degree is greater than 0.317, the pores larger than 100 nm in the concrete increase significantly with the increase of the damage degree, indicating that the number of coarse pores in the concrete increases when the damage degree is larger.

The comparison between Figure 3 and Figure 5 shows that after wetting-drying cycles ,the distribution of gel pores with the degree of damage is similar to that of medium capillary pores before wetting-drying cycles.

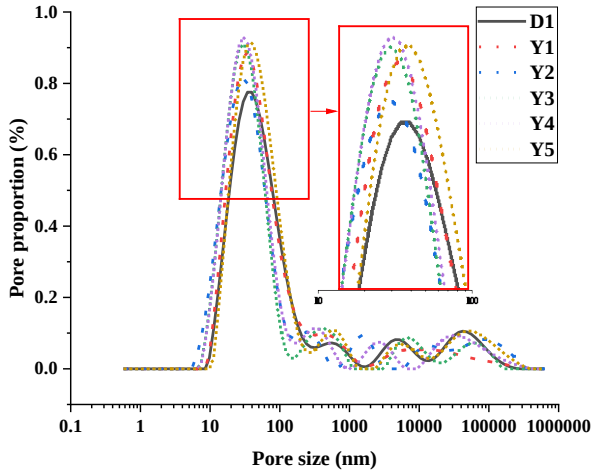

Figure 2. NMR pore distribution before drying-wetting cycles

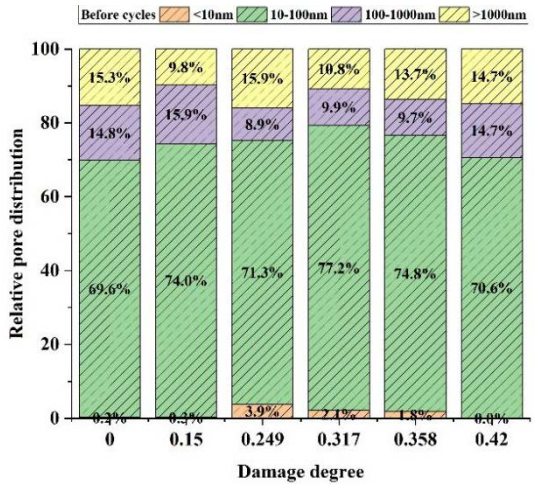

Figure 3. NMR relative pore distribution before drying-wetting cycles

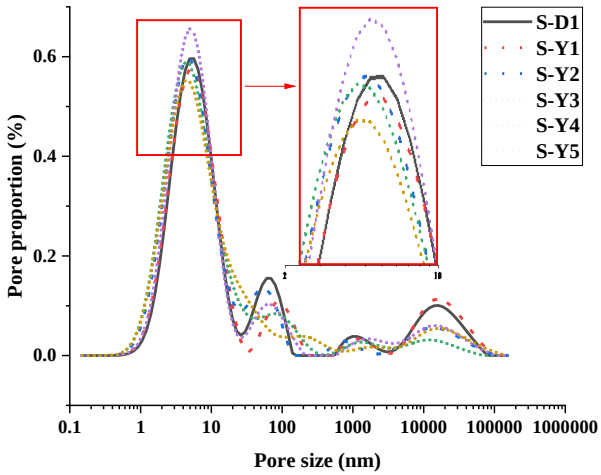

Figure 4. NMR pore distribution after drying-wetting cycles

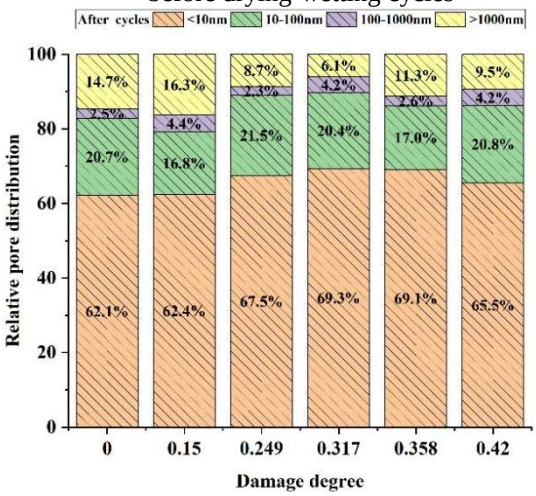

Figure 5. NMR relative pore distribution after drying-wetting cycles

3.2 Effect of Drying-wetting Cycle on Pore Structure

The comparison between Figure 2 and Figure 4 shows that after the drying-wetting cycles, the pore size distribution curve of the concrete specimen moves to the left and the peak value decreases. And the range of main pores in concrete changes from 10-1000 nm to 1-100 nm. Figure 4 shows that the maximum pore proportion of undamaged concrete specimens D1 after the drying-wetting cycles is roughly the same as that of damaged concrete specimens except S-Y4. The pore size corresponding to the maximum pore proportion is roughly within 4-6 nm, which indicates that the pore size of undamaged concrete specimens after the drying-wetting cycles is close to that of some concrete specimens with lower damage degrees. The results in Figure 3 and Figure 5 indicated that after the drying-wetting cycles, the proportion of pores with a pore size smaller than 10 nm increases significantly, while the pores with a pore size of 10-1000 nm decrease obviously. This can be explained by the blockage of some slightly larger capillary pores with a diameter of 10-1000 nm in the concrete, resulting in a larger proportion

of pores with a pore size smaller than 10 nm. This also proves that drying-wetting cycles change the internal microstructure of concrete, and promote the main pores to evolve into gel pores or small capillary pores.

After the drying-wetting cycles, the porosity changes of the specimens are shown in Table 4. After drying-wetting cycles, the porosity of all damaged concrete specimens decreased with varying degrees, indicating that the microstructure of the specimens after drying-wetting cycles will have a structural optimization process in the early stage of drying-wetting cycles. This is consistent with the decrease of porosity after drying-wetting cycles in the literature (Sun et al. 2020, Díaz et al. 2008, Yang 2019).

Table 4. Changes in porosity of specimens after drying and wetting cycles

Specimen	D1	YQ-1	YQ-2	YQ-3	YQ-4	YQ-5
Porosity before cycle（%）	12.5921	13.2080	13.0187	12.5739	13.4868	13.9005
Porosity after cycles（%）	10.8020	10.5402	11.4804	11.6156	11.9640	11.7837

3.3 Oxygen Diffusivity before and after Drying-wetting Cycle

The oxygen diffusivity of concrete specimens was obtained according to Equation (2) and Equation (3). Figure 6 shows that the oxygen diffusion coefficient of the specimen increases with the increase of the damage degree before the drying-wetting cycles. The test results are consistent with the order of magnitude of the gas diffusion coefficient obtained by other scholars (Andrade 2010). The oxygen diffusivity increases linearly with the damage degree increasing to 0.317 for concrete without drying and wetting cycles. When the damage degree is greater than 0.317, diffusivity increases faster with the damage degree. Combined with Figure 3, it can be considered that when the damage degree is greater than 0.317, as the damage degree increases, the proportion of macropores (>100 nm) in the specimen increases, thus significantly increasing the oxygen diffusion coefficient.

As shown in Figure 6, the variation of the oxygen diffusivity of concrete specimens with damage degree is not obvious after the drying-wetting cycles. After the drying-wetting cycles, the oxygen diffusivity of the damaged concrete decreases by about 3 to 7 times, and the oxygen diffusivity of the undamaged concrete decreases by about 10 times. With the increase of damage degree, the reduction effect is roughly decreasing. This is because the drying-wetting cycles optimize the internal structure of concrete, but the optimization effect is less obvious when the damage is relatively large. This may be explained by chloride binding effects (Díaz et al. 2008). After the drying-wetting cycles, the binding amount of Cl^- reaches the upper limit, and the pores cannot be filled continuously. The pore structure of concrete will not change significantly. The increase in oxygen diffusivity is mainly due to the damage of the microstructure caused by the larger damage degree before the drying-wetting cycles.

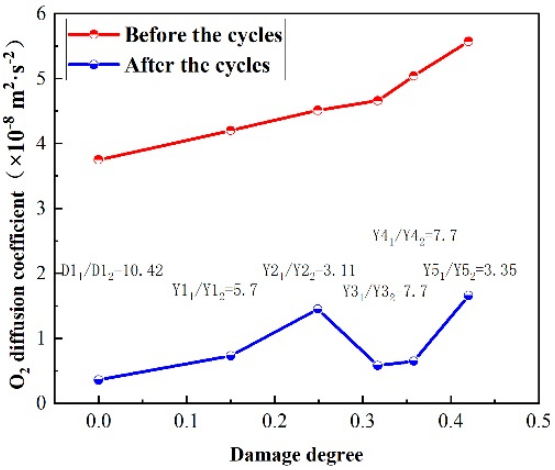

Figure 6. Variation of oxygen diffusion coefficient after drying-wetting cycles

4 Conclusion

In this paper, the oxygen diffusion of damaged concrete under axial tensile fatigue load is studied. Combined with pore size distribution, the influencing mechanism of the oxygen diffusion coefficient of the damaged concrete structure before and after the drying-wetting cycles is analyzed. The main conclusions are as follows:

- The damage degree of concrete increases with the increase of load level and is close to linear growth. The proportion of small and medium capillary pores increases first and then decreases with the increase of damage degree.
- Before and after the drying-wetting cycles, the pores of the damaged concrete and the undamaged concrete specimens are distributed in the range of 1-100 nm. After the drying-wetting cycles, the pore size distribution curve of the concrete specimen moves to the left and the peak value decreases, and the proportion of gel pores increases significantly, and the proportion of medium and large capillary pores decreases. The porosity of all damaged concrete specimens decreased after drying-wetting cycles, indicating that the microstructure of the specimens after drying-wetting cycles will have a structural optimization process in the early stage of drying-wetting accelerated erosion, presenting as the main pores evolve into gel pores or small capillary pores.
- The oxygen diffusion coefficient of the specimen increases with the increase of damage degree. After the drying-wetting cycles, the oxygen diffusion coefficient of different damaged concrete decreases, and the oxygen diffusion coefficient of undamaged concrete decreases most significantly, nearly 10 times. With the increase of damage degree, the reduction effect is generally decreasing.

References

Andrade, C. (2010). *Types of Models of Service Life of Reinforcement: The Case of the Resistivity*. 1.

Dhir, R.K., Hewlett, P.C., Byars, E.A., and Shaaban, I.G. (1995). *A new technique for measuring the air permeability of near-surface concrete.* Magazine of Concrete Research, 47(171), 167–176. https://doi.org/10.1680/macr.1995.47.171.167

Díaz, B., Freire, L., Merino, P., Nóvoa, X.R. and Pérez, M.C. (2008). *Impedance spectroscopy study of saturated mortar samples*. Electrochimica Acta, 53(25), 7549–7555. https://doi.org/10.1016/j.electacta.2007.10.042

Fu, C., Ye, H., Jin, X., Yan, D., Jin, N., and Peng, Z. (2016). *Chloride penetration into concrete damaged by uniaxial tensile fatigue loading*. Construction and Building Materials, 125, 714–723. https://doi.org/10.1016/j.conbuildmat.2016.08.096

He, C. (2019). *Experimental study on chloride transport and oxygen diffusion of cementitious materials with considering the interfacial transition zone* [Master, Zhejiang University of Technology]. https://doi.org/10.27463/d.cnki.gzgyu.2019.000370

He, R., Ma, H., Hafiz, R.B., Fu, C., Jin, X., and He, J. (2018). *Determining porosity and pore network connectivity of cement-based materials by a modified non-contact electrical resistivity measurement: Experiment and theory*. Materials and Design, 156, 82–92. https://doi.org/10.1016/j.matdes.2018.06.045

Huang, Y., Ye, H., Fu, C., and Jin, N. (2017). *Modeling moisture transport at the surface layer of fatigue-damaged concrete.* Construction and Building Materials, 151, 196–207. https://doi.org/10.1016/j.conbuildmat.2017.06.038

Kurumatani, M., Anzo, H., Kobayashi, K., Okazaki, S., and Hirose, S. (2017). *Damage model for simulating chloride concentration in reinforced concrete with internal cracks*. Cement and Concrete Composites, 84, 62–73. https://doi.org/10.1016/j.cemconcomp.2017.08.015

Luo, D. and Niu, D. (2019). *Influences of water-to-cement ratio and curing condition on water absorption of internal curing concrete*. Journal of Building Structures, 40(1), 165–173. https://doi.org/10.14006/j.jzjgxb.2019.01.019

Niu, D., Huang, D., Zheng, H., Su, L., Fu, Q., and Luo, D. (2019). *Experimental Study on Mechanical Properties and Fractal Dimension of Pore Structure of Basalt–Polypropylene Fiber-Reinforced Concrete.* Applied Sciences, 9(8), 1602. https://doi.org/10.3390/app9081602

Sun, L.F., Jiang, K., Zhu, X., and Xu, L. (2020). *An alternating experimental study on the combined effect of freeze-thaw and chloride penetration in concrete*. Construction and Building Materials, 252, 119025. https://doi.org/10.1016/j.conbuildmat.2020.119025

Types of models of services life of reinforcement: The case of the resistivity. (2009).

Wang, H., Dong, Y., Sun, X. and Jin, W. (2012). *Damage mechanism of concrete deteriorated by sulfate attack in wet-dry cycle environment*. Journal of Zhejiang University (Engineering Science), 46(07), 1255–1261.

Wei, J., Li, S., Dong, R., Liu, X. and Wu, Z. (2016). *Fatigue damage constitutive model of concrete considering effect of residual deformation*. Journal of Hunan University (Natural Science), 43(07), 57–61.

Yadav, I.N., and Thapa, K.B. (2020). *Fatigue damage model of concrete materials*. Theoretical and Applied Fracture Mechanics, 108, 102578. https://doi.org/10.1016/j.tafmec.2020.102578

Yang, M. (2019). *Experimental study on concrete attacked by sulfate corrosion under different dry-wet cycles* [Master, Zhengzhou University]. https://kns.cnki.net/kcms2/article/abstract?v=3uoqIhG8C475KOm_zrgu4lQARvep2SAkOsSuGHvNoCRcTRpJSuXuqd3vAsxhwkN7Q1oYPN9QUNsY60Rbp8uliXejyJJWBdJJanduniplatform=NZKPT

Zhang, J., Bian, F., Zhang, Y., Fang, Z., Fu, C., and Guo, J. (2018). *Effect of pore structures on gas permeability and chloride diffusivity of concrete*. Construction and Building Materials, 163, 402–413. https://doi.org/10.1016/j.conbuildmat.2017.12.111

Zhang, J., Li, D., Chen, W., Wang, J. and Gao, Y. (2016). *Relationship between time-variability of chlorion diffusion in concrete and pore fractal characteristic under tidal range environment*. Journal of Natural Disasters, 25(6), 51–57. https://doi.org/10.13577/j.jnd.2016.0607

Zhou, L., Jin, N., Fu, C., Tian, Y. and Jiang, H. (2018). *Prediction model of oxygen diffusion in cement-based materials under dry condition*, Journal of the Chinese Ceramic Society, 46(08), 1133–1140. https://doi.org/10.14062/j.issn.0454-5648.2018.08.13

Zhou, R., Li, Q., Wang, J., Zhou, K., He, R., and Fu, C. (2021). *Assessment of Electrical Resistivity and Oxygen Diffusion Coefficient of Cementitious Materials from Microstructure Features.* Materials, 14(12), 3141. https://doi.org/10.3390/ma14123141

Zhu, J. (2003). *Experimental study on fatigue properties of plain concrete under biaxial stress states and theories on failure prediction* [Doctor, Dalian University of Technology]. https://kns.cnki.net/kcms2/article/abstract?v=3uoqIhG8C447WN1SO36whBaOoOkzJ23ELn_-3AAgJ5enmUaXDTPHrNEyxIlD3f72vUiEAU48nmSn_5_4m_Dwf8_PjH5BSpT-anduniplatform=NZKPT